Journal of Membrane Science
Volume 555, June 2018, pp. 125-133
DOI:10.1016/j.memsci.2018.03.032

Identification of gas sparging regimes for granular anaerobic membrane bioreactor to enable energy neutral municipal wastewater treatment

K.M. Wang[a], D. Cingolani[b], A.L. Eusebi[b], A. Soares[a], B. Jefferson[a], E.J. McAdam[a*]

[a]Cranfield Water Science Institute, Vincent Building, Cranfield University, Bedfordshire, MK43 0AL, UK
[b]Department of Materials, Environmental Sciences and Urban Planning (SIMAU), Università Politecnica delle Marche, 60131, Ancona, Italy

Abstract

In this study, conventional and novel gas sparging regimes have been evaluated for a municipal wastewater granular anaerobic MBR to identify how best to achieve high sustainable fluxes whilst simultaneously conserving energy demand. Using continuous gas sparging in combination with continuous filtration, flux was strongly dependent upon shear rate, which imposed a considerable energy demand. Intermittent gas sparging was subsequently evaluated to reduce energy demand whilst delivering an analogous shear rate. For a flux of 5 L m^{-2} h^{-1}, a fouling rate below 1 mbar h^{-1} was sustained with low gas sparging frequency and gas sparging rates. However, to sustain low fouling rates for fluxes above 10 L m^{-2} h^{-1}, a gas sparging frequency of 50 % (i.e. 10 s on/10 s off) and an increase in gas sparging rate is needed, indicating the importance of shear rate and gas sparging frequency. An alternative gas sparging regime was subsequently tested in which filtration was conducted without gas sparging, followed by membrane relaxation for a short period coupled with gas sparging, to create a *pseudo* dead-end filtration cycle. Fouling characterisation evidenced considerable cake fouling rates of 200-250 mbar h^{-1} within each filtration cycle. However, long term fouling transient analysis demonstrated low residual fouling resistance, suggesting the cake formed during filtration was almost completely reversible, despite operating at a flux of 15 L m^{-2} h^{-1}, which was equivalent or higher than the critical flux of the suspension. It is therefore asserted that by operating filtration in the absence of shear, fouling is less dependent upon the preferential migration of the sub-micron particle fraction and is instead governed by the compressibility of the heterogeneous cake formed, which enables higher operational fluxes to be achieved. Comparison of energy demand for the three gas sparging regimes to the energy recovered from municipal wastewater AnMBR demonstrated that only by using dead-end filtration can energy neutral wastewater treatment be realised which is the ultimate ambition for the technology.

Keywords: *MBR, gas bubbling, hydrodynamics, energy neutral, domestic, sewage*

1. Introduction

Electricity demand in the water industry accounts for 2-3% of national power production [1]. More than half of this demand is for aeration in activated sludge [2,3]. Anaerobic processes therefore present an attractive alternative to conventional aerobic domestic wastewater treatment since there is no aeration, less sludge production and energy can be recovered from the biogas formed [4,5]. The energy saved through aeration coupled with the potential for energy production, offers the prospect of energy neutral sewage treatment, which is the ultimate ambition for many advocates of this technology [6].

For municipal application, the main challenge for conventional anaerobic technology is preventing biomass washout [4]; an effect which is exacerbated at low temperature [7]. In anaerobic membrane bioreactors (AnMBRs), the membrane enables complete biomass retention, thereby facilitating the separation of hydraulic retention time (HRT) from solids retention time (SRT) [8–10]. Furthermore, membrane integration can deliver permeate compliant for chemical oxygen demand (COD) and suspended solids [10] in addition to a reduced biological oxygen demand (BOD_5). Whilst the membrane enables process intensification, the AnMBR matrix is concentrated, and considerably more heterogeneous than conventional aerobic MBR which increases fouling propensity and reduces the attainable flux [11]. As such fouling mitigation contributes over two-thirds of the overall energy demand for immersed AnMBR [12], which emphasises the need for fouling control strategies that limit AnMBR membrane fouling whilst conserving energy [5,13]. Our previous anaerobic research on municipal wastewater with an average temperature of 18 °C [14], demonstrated that 0.28 kWh m^{-3} energy is recoverable from biogas and dissolved methane, which is comparable to the average energy production of 0.34 kWh m^{-3} cited for AnMBR treating settled municipal wastewater in the literature [8,14–16]. For comparison, the specific energy demand for membrane operation of full-scale aerobic MBR is typically between 0.19 and 0.70 kWh m^{-3} [17]. Consequently, the specific energy demand for AnMBR membrane operation must be towards the lower end of the energy demand range for conventional aerobic MBR to achieve energy self-sufficiency, despite operating in a more challenging matrix [11] (Figure 1).

Immersed membranes are predominantly studied for inclusion within AnMBR due to their lower specific energy demand, with gas sparging employed for fouling mitigation [9,13,18]. Analogous gas sparging regimes to those of aerobic MBR are commonly employed

in AnMBR studies, comprising of either continuous gas sparging (CGS) or intermittent gas sparging (IGS, 10 s on/10 s off) in which cycling enables analogous shear stress at the membrane wall, whilst enabling a 50% reduction in energy demand [4,5,8,15,19,20]. Several AnMBR studies have now evidenced that integrating immersed membranes within Upflow Anaerobic Sludge Blanket (UASB) configured AnMBR [5,11,21,22] develop less tenacious fouling than within Completely Stirred Tank Reactor (CSTR) configured AnMBR. The authors accounted for this by the considerably lower solids concentration developed within the membrane tank, which evidently limited cake layer growth at the membrane surface [9,22,23]. Using a UASB configured AnMBR, Martin-Garcia et al. [5] undertook a preliminary investigation of an alternative gas sparging regime which comprised sequential filtration cycles without gas sparging, followed by a combination of backwash and gas sparging, to create a low energy pseudo dead-end (DE) filtration cycle [24]. The authors determined reasonable sustainable flux of 7 L m^{-2} h^{-1} despite undertaking filtration in the absence of shear, which considerably reduced the gas sparging requirement and corroborates findings of earlier investigation into pseudo dead-end (DE) filtration for MBR with low solids concentration [24,25].

To the best of our knowledge, there have been no previous studies that have explicitly sought to establish whether the gas sparging regimes employed in MBR literature can sustain flux using less energy than produced by an AnMBR treating domestic wastewater. Such investigation is critical to establishing whether the transition to energy neutral wastewater treatment is achievable. The aim of this study is therefore to critically evaluate conventional (continuous and intermittent) and non-conventional gas sparging regimes (pseudo dead-end) within UASB configured AnMBR, to identify controlling parameters that govern sustained permeability within each gas sparging regime whilst simultaneously identifying their capacity to deliver energy neutral operation. Specific objectives are to: (i) identify which parameters govern sustained operation for each gas sparging regime; (ii) compare fouling behaviours under different gas sparging regimes; and (iii) identify the most feasible gas sparging regime for delivering sustained membrane operation with minimum energy demand.

2. Material and methods

2.1 Anaerobic MBR pilot plant

The AnMBR consisted of a granular UASB (G-UASB) followed by a separate membrane tank. The 42.5 L cylindrical UASB was constructed of Perspex and fitted with a lamella plate clarifier for solid/liquid/gas separation (Paques, Balk, The Netherlands) (Figure 2). The UASB was seeded with 16 L of granular sludge sourced from a mesophilic UASB used for the pulp and paper industry. Settled sewage from Cranfield University's sewage works was fed to the base of the UASB with a peristaltic pump (520S, Watson Marlow, Falmouth, UK). Average sewage temperature was 16.3±3.7 ˚C. The UASB was operated at a HRT of 8 h and allowed to acclimate for 360 days prior to this experiment. The upflow velocity was maintained at 0.8-0.9 m h^{-1} which provided bed expansion to around 40% of total column height. Due to the bed expansion, the light sludge fraction (dispersed growth from the influent) accumulated in a layer above the granular bed [26,27], and was withdrawn on occasion once washout into the downstream membrane tank was noted by an increase in suspended solids concentration. No granular biomass was withdrawn from the G-UASB during the 400-day trial.

Effluent from the UASB overflowed into a 30 L cylindrical membrane tank (0.17 m diameter x 1.25 m height) (Figure 2). The retentate was recycled from the membrane tank to the bottom of the UASB which helped sustain the upflow velocity. The membrane module (ZW-10) (GE Water & Process Technologies, Trevose, USA) comprised four elements each of which consisted of 54 polyvinylidene fluoride (PVDF) hollow fibres (0.72 m in length and 1.9 mm outer diameter) with a nominal pore size of 0.04 µm, providing a total surface area of 0.93 m^2. Fibre looseness was around 5% in accordance with manufacturer specification. Permeate was extracted by a peristaltic pump (520U, Watson Marlow, Falmouth, UK). Pressure transducers were sited on the permeate line (-1 to 1 bar, PMC 131, Endress + Hauser, Manchester, UK) and at the base of the membrane tank (0-2.5 bar, 060G2418, Danfoss, Nordborg, Denmark) to measure transmembrane pressure (TMP) and liquid level height respectively. Nitrogen-enriched air was produced by a nitrogen generator (NG6, Noblegen gas generator, Gateshead, UK) for gas sparging. During DE operation, filtration was conducted without gas sparging, followed by membrane relaxation for a short period coupled with gas sparging. The introduction of gas sparging between filtration cycles was controlled using a solenoid valve (Type 6014, Burkert, Ingelfingen, Germany) connected

to a multifunction timer relay (PL2R1, Crouzet, Valence, France). Specific gas demand per unit membrane area (SGD_m) was controlled by needle valve (Key Instruments, Langhorne, US). At a SGD_m of 2.0 m^3 m^{-2} h^{-1}, the shear stress intensity imparted through gas sparging bubbling corresponds to a gas velocity gradient of around 460 s^{-1} [25,28]:

$$G = \left(\frac{Q_a g h}{V_T \nu_a}\right)^{0.5} \quad (1)$$

where Q_a is gas flow-rate (m^3 s^{-1}), g is gravity constant (m s^{-2}), h is fluid height (m), V_T is reactor volume (m^3) and ν_a is the apparent kinetics viscosity (m^2 s^{-1}). ν_a can be calculated from dynamic viscosity (μ, Pa s) by $\nu_a = \mu/\rho$, where ρ is density (kg m^{-3}).

Critical flux (J_C) analysis was conducted with the flux step method [29] using flux steps of 3 L m^{-2} h^{-1}, with a step duration of 10 minutes. The trials were conducted in batch and permeate recycled back to the membrane tank. To establish reproducibility, critical flux trials were conducted in triplicate at an SGD_m of 2.0 m^3 m^{-2} h^{-1}. At 15 L m^{-2} h^{-1}, a relative standard deviation for TMP of 3.6 % was recorded. Gas sparging regimes were compared through trials conducted to 24 h filtration, or where TMP reached a maximum of 550 mbar. Water flux was normalised to 20 °C (J_{20}) according to [17]:

$$J_T = J_{20} \cdot 1.025^{(T-20)} \quad (2)$$

where J_T is permeate flux at T °C, J_{20} is the permeate flux normalised to 20 °C, T is temperature (°C). Analysis was undertaken in triplicate at fixed conditions to ascertain reproducibility after 24 h (CGS, J_{20}= 13.5 L m^{-2} h^{-1}, SGD_m= 2.0 m^3 m^{-2} h^{-1}), and a relative standard deviation for TMP of 7.6 % identified. The threshold for sustainable membrane operation was fixed to fouling rate (d*P*/dt) of <1 mbar h^{-1} over 24 h which corresponds to the d*P*/dt determined for sub-critical flux operation within full-scale municipal aerobic MBR [30] and is coincident with the d*P*/dt observed in this study for TMP trends characterised by a 'flat' temporal profile.

Dead-end filtration cycle analysis was undertaken using three profile characteristics [31]. The initial TMP for each filtration cycle (TMP_i) which is related to the resistance provided by the clean membrane (R_m) and the internal residual fouling resistance (R_{if}) which is not removed by physical cleaning:

$$TMP_i = J.\mu.(\mathrm{R_m} + \mathrm{R_{if}}) \quad (3)$$

where J is the permeate flux (L m^{-2} h^{-1}). Within the filtration cycle, fouling originates from cake formation which can generally be characterised by a linear increase in TMP, with the slope defined as the cake fouling rate (r_f):

$$TMP = r_f.t + TMP_i \quad (4)$$

According to the cake filtration model, the TMP can also be described through inclusion of suspension characteristics [32]:

$$TMP = TMP_i + \Delta TMP_c = TMP_i + \mu\alpha\varpi J^2 t \quad (5)$$

where ΔTMP_c is the pressure drop of the cake layer (Pa), α is specific cake resistance (m kg^{-1}), ω is the solids concentration in the cake per unit filtrate volume (assuming similar to MLSS concentration in the bulk sludge, kg m^{-3}). The cake compressibility can be described when filtering microbial suspensions [33]:

$$\alpha = \alpha_0(1 + \frac{\Delta TMP_c}{P_a}) \quad (6)$$

where α_0 is the specific cake resistance at zero pressure and P_a is the pressure required to obtain a specific cake resistance twice as high as α_0. The critical mass ($M_{critical}$) during the dead-end cycle is related to the critical filtered volume (V_{crit}) and MLSS concentration in the bulk sludge:

$$M_{critical} = V_{crit} \cdot C_b \quad (7)$$

After each test, the membrane was rinsed with tap water and chemically cleaned in 500 mg L^{-1} sodium hypochlorite for 3 h. During this period, a spare module was introduced to maintain constant AnMBR operation. After chemical cleaning, the module was rinsed with tap water and the clean water permeability assessed to assure recovery before reuse. Over the duration of assessment, clean water permeability varied by less than 10%.

For the specific energy demand, only the blower for the gas sparging was considered and calculated by applying Equation (8-10) [2]:

$$P_{power} = \frac{\mathrm{w} \cdot \mathrm{R} \cdot \mathrm{T_1}}{29.7 \cdot \mathrm{n} \cdot \mathrm{e}}\left[\left(\frac{\mathrm{P_2}}{\mathrm{P_1}}\right)^{0.283} - 1\right] \quad (8)$$

$$w = \frac{SGD_m \cdot A \cdot \rho_G}{3600} \quad (9)$$

$$W = \frac{P_{power} \cdot 1000}{J_{20} \cdot A} \quad (10)$$

where P_{power} is power requirement (kW); w is weight of flow of gas (kg s^{-1}); P_1 is inlet pressure (1.01x10^5 Pa); P_2 is outlet pressure (assuming 3 m hydraulic head, 1.3 x10^5 Pa); T_1 is

inlet temperature (K, assuming 293 K); n = (k-1)/k; k=1.4 for nitrogen in this case; e is compressor efficiency (0.8); A is membrane surface area (m^2); ρ_G is the gas density (1.165 kg m^{-3} for nitrogen); W is the specific energy demand (kWh m^{-3}).

2.2 Analytical methods

Mixed liquor suspended solids (MLSS) and biological oxygen demand (BOD_5) were measured according to Standard Methods [34]. Total and soluble COD were analysed with Merck test kits (Merck KGaA, Darmstadt, Germany). Soluble COD was measured after filtering with a 1.2 µm filter paper (70mm Glass Fibre Filter Paper Grade GF/C, Whatman, GE Healthcare Life Sciences, Little Chalfont, UK). Particle size was measured by integrated laser diffractor (Mastersizer 3000, Malvern Instruments Ltd, Malvern, UK). Acetate was quantified using high performance liquid chromatography (HPLC) (Shimadzu HPLC Class VP series, Kyoto, Japan) with a Rezex ROA/Organic Acid 7.80 mm x 300 mm column (Phenomenex, Macclesfield, UK) [35]. Protein and carbohydrate concentrations were measured using the modified Lowry method ($UV_{750\,nm}$) [36] and Dubios phenol sulphuric acid method ($UV_{490\,nm}$) [37] respectively. Bovine serum albumin (BSA) (Sigma-Aldrich, UK) and D-glucose (Acros Organics, UK) were used as the standard reference for protein and carbohydrates respectively. Samples were taken from the membrane tank for analyses. All analyses were undertaken in triplicate.

3. Results

3.1 Anaerobic MBR characterisation and critical flux determination

Consistently low effluent total COD (COD_t) and BOD_5 of 41±16 and 11±7 mg L^{-1} were achieved during 400 days operation (Table 1), which is comparable to an earlier study of AnMBR operated on the same sewage [5], demonstrating stable process performance throughout the study. Acetate was not detected in the permeate (<2.0 mg L^{-1}), which illustrates good utilisation of the soluble substrate. The membrane tank was characterised by average MLSS of 384±190 mgMLSS L^{-1} and soluble microbial products (SMP) concentration of 149±65 mg COD L^{-1} (Table 1). The SMP concentration expressed as a sum of protein and carbohydrate was 78±28 mg L^{-1}, and was characterised by a protein/ carbohydrate ratio (SMP P/C) of 3.8. Median particle size (d_{50}) of 62±45 µm was observed in the membrane tank. For SGD_m of 0.2 to 2.0 $m^3\ m^{-2}\ h^{-1}$, fouling rate (dP/dt) was similar across

the initial flux steps applied during critical flux (J_c) analysis (Figure 3). However, following a progressive increase in flux, dP/dt began to increase which indicated the weak form of the J_c to lie between 12 and 15 L m^{-2} h^{-1} for the AnMBR suspension at a SGD_m of 2.0 m^3 m^{-2} h^{-1}. For comparison, J_c for a SGD_m of 0.5 m^3 m^{-2} h^{-1} was between 9 and 12 L m^{-2} h^{-1}.

3.2 Continuous filtration and continuous gas sparging

The impact of flux on fouling rate was assessed using a fixed SGD_m of 0.2 m^3 m^{-2} h^{-1} (Figure 4). At J_{20} *of* 5 L m^{-2} h^{-1}, d*P*/dt was below 1 mbar h^{-1}. However, with an increase in flux, d*P*/dt increased considerably, and for J_{20} exceeding 10 L m^{-2} h^{-1}, the TMP reached the maximum TMP (TMP_{max}, 550 mbar) in less than 24 h. The impact of SGD_m was subsequently evaluated at J_{20} of 13.5 L m^{-2} h^{-1}(Figure 4). When SGD_m increased from 0.1 to 1.0 m^3 m^{-2} h^{-1}, d*P*/dt decreased from 224 to less than 1 mbar h^{-1}. Upon increasing SGD_m further from 1.0 to 2.0 m^3 m^{-2} h^{-1}, a decrease in d*P*/dt was not noted, indicating a plateau had been reached.

3.3 Continuous filtration and intermittent gas sparging

To reduce net energy demand, gas sparging frequency ($\Theta_{gs,f}$) was evaluated for J_{20} *of* 5, 10 and 13.5 L m^{-2} h^{-1} (Figure 5):

$$\Theta_{gs,f} = \frac{\theta_{gs,on}}{(\theta_{gs,on}+\theta_{gs,off})} \quad (11)$$

For this analysis, gas sparging on time ($\theta_{gs,on}$) was fixed at 10 s and gas sparging off time ($\theta_{gs,off}$) varied from 10 to 90 s. At the lowest J_{20} of 5 L m^{-2} h^{-1}, d*P*/dt of less than 1 mbar h^{-1} was achieved for all conditions except when SGD_m and $\Theta_{gs,f}$ were reduced to 0.2 m^3 m^{-2} h^{-1} and 10% respectively. For J_{20} of 10 and 13.5 L m^{-2} h^{-1}, a d*P*/dt of less than 1 mbar h^{-1} was only achieved when $\Theta_{gs,f}$ was fixed at 50% and SGD_m was at least 1.0 m^3 m^{-2} h^{-1}. The impact of extending $\theta_{gs,on}$ was subsequently evaluated (Figure 6). Whilst increasing gas sparging frequency ($\Theta_{gs,f}$) reduced d*P*/dt with an applied $\theta_{gs,on}$ of 30 s, d*P*/dt remained higher than when operating with a $\theta_{gs,on}$ of 10 s. Under the same $\Theta_{gs,f}$ of 50 %, higher ($\theta_{gs,on}$) with gas sparging 30 s on/30 s off had higher d*P*/dt than gas sparging 10 s on/10 s off.

3.4 Pseudo dead-end filtration using intermittent filtration and intermittent gas sparging

The impact of SGD_m and flux were investigated using pseudo DE filtration (Figure 7). Each filtration cycle (9 mins.) was conducted without gas sparging, and was then followed by a combination of membrane relaxation and gas sparging for one minute. To compensate for the lost productivity introduced by membrane relaxation, the actual flux was increased to provide a net flux comparable to the other gas sparging regimes. For example, an actual J_{20} of 15 L m^{-2} h^{-1} was used to achieve a net flux ($J_{20\ net}$) of 13.5 L m^{-2} h^{-1}. A low fouling rate of below 1 mbar h^{-1} was achieved at $J_{20\ net}$ of 5 L m^{-2} h^{-1} when SGD_m was above 0.5 m^3 m^{-2} h^{-1} and at $J_{20\ net}$ of 10 L m^{-2} h^{-1} when SGD_m was above 1.0 m^3 m^{-2} h^{-1}. Interestingly, a fouling rate of less than 1 mbar h^{-1} was also recorded at 13.5 L m^{-2} h^{-1} when an SGD_m of 2.0 m^3 m^{-2} h^{-1} was used. Since gas sparging was introduced for only one minute in a ten minute cycle, a SGD_m of 2.0 m^3 m^{-2} h^{-1}, corresponded to a net SGD_m ($SGD_{m,net}$) of 0.2 m^3 m^{-2} h^{-1}. The impact of gas sparging time was subsequently evaluated which is analogous to the membrane relaxation period (Figure 8a). Provided gas sparging was at least one minute in length, d*P*/dt was limited to less than 1 mbar h^{-1}. Filtration cycle length was also studied (Figure 8b). Increasing filtration cycle length greater than 9 mins. appeared detrimental to membrane performance. Further diagnostic investigation evidenced that the cake fouling rate (r_f) was around 200-250 mbar h^{-1} when filtration cycle length was between four and nine minute (Figure 9). However, despite this considerable 'in-cycle' fouling rate, provided filtration cycle length was below 9 mins., negligible increase in residual fouling resistance (R_{if}) was noted. In contrast, for a 14 mins. filtration cycle length, both r_f and R_{if} increased to 400 mbar h^{-1} and 3 x 10^{12} m^{-1} respectively.

4. Discussion

In this study, a *pseudo* dead-end gas sparging regime has been identified that can deliver sustained membrane operation using a fraction of the energy demanded for conventional gas sparging strategies. Comparison of the various gas sparging strategies employing the same net energy demand (0.13 kWh m^{-3}, Figure 10) evidences that: (i) shear stress (G=460 s^{-1}) is critical to sustaining permeability during continuous gas sparging, such that equivalent low energy operation cannot be achieved; (ii) intermittent gas sparging (10s on/10s off) cannot sustain permeability when gas sparging rate is reduced to normalise energy use; and (iii) filtration without shear stress, as used in pseudo dead-end operation, enables sustained

operation (no. 3, Table 2) analogous to that observed with continuous gas sparging, but using only a fraction of the energy [25]. During continuous gas sparging (CGS), d*P*/dt increased when flux increased at a fixed SGD_m and decreased when SGD_m was increased at a fixed flux (Figure 4). This is analogous to the J_c analysis (Figure 3), and demonstrates the importance of shear stress under CGS. At a J_{20} of 13.5 L m^{-2} h^{-1}, a plateau in fouling rate was achieved above a SGD_m of 1.0 m^3 m^{-2} h^{-1}, from which an optimum operating condition can be inferred (Figure 4). This is similar to earlier studies of CGS in both aerobic and anaerobic MBR [4,30]; although the SGD_m required to achieve a plateau, is specific to the suspension characteristics. In a study of particle deposition within model binary dispersions, Krompcamp et al. [38] identified that only the small particles deposited at the membrane surface as they had a lower J_c. In this study, the considerable specific gas demand required to achieve this plateau at modest fluxes, relative to conventional aerobic MBR, can be ascribed to the matrix composition in AnMBR which comprises of concentrated biopolymers with a more disperse particle distribution, fostering a lower J_c for the suspension (Table 1). McAdam et al. [25] reported that through continuous gas sparging, median particle size (d_{50}) decreased from 182 µm, observed during DE gas sparging, to 52 µm. Consequently, the additional shear stress introduced with high SGD_m could lead to the propagation of more fine particles [25], with a lower J_c. Whilst sustaining continuous gas sparging at the membrane wall limits deposition of coarse particles, preferential deposition of soluble and colloidal biopolymers then occurs since their back-transport is mainly governed by Brownian rather than shear-induced diffusive effects [24,25,39]. We assert that the modest fluxes achieved for AnMBR in CGS mode are due to the preferential deposition of SMP [25], an effect which is exacerbated in AnMBR since SMP_{COD} is at least 1.5 times higher than conventional aerobic MBR (Table 1) [11].

During intermittent gas sparging (IGS), a SGD_m greater than 1.0 m^3 m^{-2} h^{-1}, and a gas sparging frequency ($\Theta_{gs,f}$) of 50 % (i.e. gas sparging 10 s on/10 s off) was sufficient to achieve the threshold fouling rate of < 1 mbar h^{-1} at 13.5 L m^{-2} h^{-1} (Figure 5). This would indicate that particle deposition within the gas sparging 'off' period is reversible during the subsequent gas sparging 'on' period, provided sufficient shear-rate is applied [40]. In comparison to CGS, IGS with a 10 s on/10 s off sparging cycle, provides a 50% energy saving whilst enabling similarly sustainable fluxes [41]; such methodologies have been

commercially realised in aerobic MBR for municipal wastewater treatment [42]. A lower $\Theta_{gs,f}$, which indicates a longer gas sparging off time ($\theta_{gs,off}$) led to d*P*/dt greater than 1 mbar h^{-1} (Figure 5 and Figure 6), which has been similarly demonstrated elsewhere [13]. When adopting the same $\Theta_{gs,f}$ of 50%, the longer gas sparging period ($\theta_{gs,on}$, 30 s on) provided higher d*P*/dt when compared with $\theta_{gs,on}$ of 10 s (Figure 6). Similarly, Guibert et al. [43] also demonstrated higher dP/dt when applying a 60 s on/60 s off air sparging cycle compared with 15 s on/15 s off in an aerobic MBR. The authors proposed that the permeability decline was due to prolonged filtration periods without shear, that was no longer restorative following gas sparge inclusion. Consequently, IGS is limited to a 10s on/ 10s off cycle ($\Theta_{gs,f}$, 50%) to yield a maximum energy saving of 50% at 13.5 L m^{-2} h^{-1} versus CGS.

Characterisation of individual filtration cycles within the dead-end regime, demonstrated significant cake fouling rates (r_f) of 200-250 mbar h^{-1} (Figure 9). However, provided the filtration cycle was fixed to below 9 mins., low fouling rate (<1 mbar h^{-1}) (Figure 8) and negligible internal residual fouling resistance (R_{if}) (Figure 9) was observed, which suggests that the cake developed during filtration can be reversed by the simultaneous use of gas sparging and relaxation introduced at the end of each filtration cycle. This is ostensibly similar to an earlier investigation of pseudo dead-end filtration for application in low solids concentration MBR for groundwater denitrification which comprised of dispersed growth biomass (0.5 to 1.1 g L^{-1}) [24,25]. Although similar in solids concentration to this study (0.4 gMLSS L^{-1}) (Table 1), AnMBR has a more complex bulk sludge matrix than denitrification and aerobic MBR, comprising of more high molecular weight colloidal matter. The authors proposed that deposit reversibility could be accounted for through the critical mass concept first proposed by Harmant and Aimar [44] in which the permeation drag force within the first layer of the loose cake increased as layer number increased, thereby increasing deposit mass until a critical value was reached which induced aggregation and collapse into a compacted cake layer [24,25]. In their study, a mono-disperse colloidal suspension was employed, with a narrow size distribution within a controlled ionic environment, which then enabled the 'critical mass' that induced collapse to be described through discrete surface force interactions [44,45]. Whilst the particle matrix within heterogeneous MBR systems, is regarded as too complex to be only described

by discrete surface forces, a transition from limited to significant irreversible fouling was observed when cycle length increased from 9 to 14 mins, which corresponded to a critical mass (Equation 7) between 0.7 and 1.1 g MLSS m^{-2} at J_{20} of 13.5 L m^{-2} h^{-1}. Vera et al. [32] described reversibility of the deposit formed within the dead-end filtration cycle of an MBR to be also governed by cake compressibility, which we propose to be dependent upon the matrix composition and character. To illustrate, in this study, the critical mass was considerably lower than previously identified for MBR (4.6-4.8 g MLSS m^{-2}, J= 24 L m^{-2} h^{-1}), which can be explained by the higher colloidal fraction within the AnMBR suspension as the SMP concentration (sum of protein and carbohydrate) (Table 1) was around 5-7 times that in denitrification MBR [24,25]. A high SMP P/C ratio of 3.8 was also obtained in this study compared with 0.6-2.1 in denitrification MBR [24,25]; a higher P/C ratio having been linked to greater fouling propensity due to the greater probability for adhesion by the protein-rich fraction, which is generally regarded as more hydrophobic than carbohydrate [46]. Specific cake resistance (α) of 10^{13-14} m kg^{-1} was estimated from filtration cycle analysis (Equation 5 and Equation 6). For illustration, , this is higher than been previously reported for cake formed by microbial floc (10^{12}-10^{13} m kg^{-1}) and similar to that of a cohesive gel layer (10^{14} m kg^{-1}) [47]. McAdam and Judd [24] demonstrated a less clear transition from non-fouling to fouling conditions when evaluating dead-end cycle length at increasing SRTs, which was ascribed to the lower colloidal contribution in the matrix; although it was also recognised that this transition would be dependent upon both suspension characteristics (such as size, charge [44] and shape [45]) as well as particle-particle and particle-membrane interactions. Whilst this conceptually supports the development of a more cohesive cake when applying dead-end filtration to AnMBR it is important to recognise that the cake formed was almost completely reversible provided cycle time was limited to around 9 mins at $J_{20\,net}$ of 13.5 L m^{-2} h^{-1}.

To achieve a net productivity with $J_{20\,net}$ of 13.5 L m^{-2} h^{-1}, an actual J_{20} of 15 L m^{-2} h^{-1} was used for the dead-end regime (Table 2). This is higher than compared with typical fluxes of 5-12 L m^{-2} h^{-1} reported in the AnMBR literature [5,31] and is equivalent to or higher than the critical flux recorded for the suspension (Figure 3). This is consistent with earlier studies of dead-end gas sparging for MBR where sustained operation was demonstrated at fluxes exceeding the critical flux [31,32]. Using continuous gas sparging, colloids undergo

preferential migration towards the membrane due to particle size segregation introduced by shear induced diffusion, whereas when dead-end filtration is undertaken, simultaneous deposition of soluble, colloidal and particulate material occurs which results in the formation of a more heterogeneous cake [25]. Consequently, dead-end filtration is apparently independent of critical flux, which suggests that higher fluxes can be achieved with considerably less energy than conventional gas sparging strategies. However, it is asserted that this strategy is only possible within low solids concentration MBR, to limit cake deposition within specific filtration cycle time (e.g. 9 mins.) (Figure 8) [24], since both the filtration time and TMP will also influence the compressibility of the cake [24,32].

For $J_{20\ net}$ of 13.5 L m^{-2} h^{-1}, the specific gas demand per unit permeate (SGD_p) was 14.8 m^3 m^{-3} with DE operation (Figure 10). Verrecht et al. [48] identified critical SGD_p of 15 and 19 m^3 m^{-3} corresponding to fluxes of 15 and 30 L m^{-2} h^{-1}, as the limit at which gas sparging energy was deployed efficiently to sustain permeability during modelling of full-scale hollow-fibre aerobic MBR. This closely corresponds to full scale municipal aerobic MBR, reportedly ranging 14 to 30 m^3 m^{-3} [40]. Consequently, the proposed dead-end gas sparging regime is comparable to the lower SGD_p threshold for aerobic MBR, despite operation within a more challenging matrix [11]. Experimental data was evaluated to identify hydrodynamic conditions capable of achieving sustained operation (dP/dt, <1 mbar h^{-1}) and benchmarked against average data for energy production from this specific wastewater (0.28 kWh m^{-3}) [14] and from the literature (0.34 kWh m^{-3}) [8,14–16] (Figure 11). In this study, it was difficult to ascertain classical gas sparging conditions that could deliver to the energy neutral proposition, whereas the dead-end gas sparging regime produced permeate at around 0.14 kWh m^{-3}, equivalent to around 50% of the energy recovered from AnMBR. Several authors have also identified that the dead-end gas sparging regime proposed can reduce the energy demand of membrane operation for niche aerobic and anoxic MBR applications[25,32]. This study provides the first comparison of dead-end gas sparging with conventional gas sparging regimes in UASB configured AnMBR. The application of DE gas sparging to AnMBR can be conceived of as considerably more challenging than previous MBR application of DE gas sparging, due to the disperse growth phase, comprising of considerable colloidal matter. Importantly, this study demonstrates that energy neutral wastewater can be achieved with AnMBR through adoption of an appropriate gas sparging

regime. An analogy can be made to LEAPmbr and MEMPULSE^{TM} innovations in aerobic MBR which sought to extend the intermittent period for gas sparging. In addition to reducing energy demand, extending intermittency reduced capital cost in aeration equipment by up to 50% [40]. Due to the increased length of the filtration cycle illustrated in this study between gas sparging cycles (around 9 mins.), it is suggested that dead-end gas sparging could therefore provide further indirect cost benefits through capital savings versus conventional MBR operation.

5. Conclusions

The UASB configured AnMBR used in this study promoted a low solids concentration local to the membrane which made the application of non-conventional hydrodynamic conditions possible. In the dead-end filtration mode, reversibility was illustrated through critical mass which is a product of solids concentration, flux and time. It is suggested that reversibility will also be dependent upon transmembrane pressure and compressibility, which will be specific to the matrix. It is important to observe that dead-end operation has now been successfully applied to three different low solids MBR applications (potable, tertiary and anaerobic municipal wastewater). Consequently, whilst the matrix will exert an influence on the practicable filtration cycle length at a prescribed flux, there is increasing evidence of the viability of this filtration mode to enable sustainable fluxes with a conservative energy demand. In this study, the highest flux tested was 15 L m^{-2} h^{-1} at which a nine minute dead-end filtration cycle was sustainable. Based on the mechanism proposed, it is suggested that higher sustainable fluxes can be achieved by reducing the filtration cycle length which warrants further study. Importantly, dead-end filtration has been shown to provide low energy membrane operation in AnMBR sufficient to achieve the aspiration of energy neutral wastewater treatment.

Acknowledgements

The authors would like to thank our industrial sponsors: Anglian Water, Scottish Water, Severn Trent Water and Thames Water for their financial and technical support.

Nomenclature

A	membrane surface area
AnMBR	anaerobic membrane bioreactor
BOD_5	five-day biological oxygen demand (mg L^{-1})
BSA	bovine serum albumin
C_b	MLSS concentrations
CGS	continuous gas sparging
COD	chemical oxygen demand (mg L^{-1})
COD_t	total chemical oxygen demand (mg L^{-1})
CSTR	completely stirred tank reactor
d_{50}	equivalent diameter corresponding to 50 % of cumulative volume undersize (μm)
e	compressor efficiency, 0.70-0.90
DE	dead-end
d*P*/dt	fouling rate (mbar h^{-1})
G-UASB	granular upflow anaerobic sludge blanket
HPLC	high performance liquid chromatography
HRT	hydraulic retention time
IGS	intermittent gas sparging
J	permeate flux (L m^{-2} h^{-1})
J_{20}	flux normalised to 20 °C
$J_{20\,net}$	net flux normalised to 20 °C
J_c	critical flux (L m^{-2} h^{-1})
J_T	flux at T °C
k	constant, k=1.4 for nitrogen
MBR	membrane bioreactor
$M_{critical}$	critical mass
MLSS	mixed liquor suspended solids
n	constant
P_1	inlet pressure (Pa)
P_2	outlet pressure (Pa)
P_a	the pressure required to obtain a specific cake resistance twice as high as α_0 (mbar)
P_{power}	power requirement (kW)
PVDF	polyvinylidene fluoride
Q_w	wastewater flow (m^3 h^{-1})
r_f	cake fouling rate (mbar h^{-1})
R	gas constant, 8.314 (J K^{-1} mol^{-1})
R_{if}	internal residual fouling resistance (m^{-1})
R_m	clean membrane resistance (m^{-1})
R_{rvf}	reversible fouling resistance (m^{-1})
R_t	total resistance (m^{-1})
SCOD	Soluble chemical oxygen demand
SGD_m	specific gas demand per unit membrane area (m^3 m^{-2} h^{-1})
$SGD_{m,\,net}$	net specific gas demand per unit membrane area (m^3 m^{-2} h^{-1})
SGD_p	specific gas demand per unit permeate (m^3 m^{-3})
SMP	soluble microbial production (mg L^{-1})
SMP_p	protein concentration (mg L^{-1})
SMP_c	carbohydrate concentration (mg L^{-1})
SMP P/C	protein to carbohydrate ratio
SRT	solids retention time
t	filtered time (min.)
T_1	temperature (K)
TMP	transmembrane pressure (mbar)
TMP_{ave}	average transmembrane pressure (mbar)
TMP_i	initial transmembrane pressure for each filtration cycle (mbar)
TMP_{max}	maximum transmembrane pressure (mbar)
TMP_t	transmembrane pressure at the end of dead-end filtration cycle (mbar)
UASB	upflow anaerobic sludge blanket
VFA	volatile fatty acid
V_{crit}	critical filtered volume (L)
W	specific energy demand (kWh m^{-3})
w	weight of flow of gas (kg s^{-1})

Greek letters

α	specific cake resistance (m kg^{-1})
α_0	specific cake resistance at zero pressure (m kg^{-1})
ΔTMP_c	pressure drop of cake layer (mbar)
$\Theta_{gs,f}$	gas sparging frequency
$\theta_{\mathrm{gs,on}}$	gas sparging on time (s)
$\theta_{gs,off}$	gas sparging off time (s)
μ	permeate viscosity (Pa s)
ρ_G	gas density (kg m^{-3})
ω	solids concentration in the cake per unit filtrate volume (kg m^{-3})

References

[1] Water UK, Wastewater Treatment and Recycling, London, UK, 2006.

[2] G. Tchobanoglous, F.L. Burton, H.D. Stensel, Wastewater Engineering Treatment and Reuse, Fourth, McGraw-Hill Companies, New York, 2004.

[3] P. Krzeminski, J.H.J.M. Van Der Graaf, J.B. van Lier, Specific energy consumption of membrane bioreactor (MBR) for sewage treatment, Water Sci. Technol. 65 (2012) 380–392.

[4] A. Robles, M.V. Ruano, F. García-Usach, J. Ferrer, Sub-critical filtration conditions of commercial hollow-fibre membranes in a submerged anaerobic MBR (HF-SAnMBR) system: the effect of gas sparging intensity, Bioresour. Technol. 114 (2012) 247–254.

[5] I. Martin Garcia, M. Mokosch, A. Soares, M. Pidou, B. Jefferson, Impact on reactor configuration on the performance of anaerobic MBRs: Treatment of settled sewage in temperate climates, Water Res. 47 (2013) 4853–4860.

[6] P.L. McCarty, J. Kim, J. Bae, Domestic wastewater treatment as a net energy producer – Can this be achieved?, Environ. Sci. Technol. 45 (2011) 7100–7106.

[7] G. Lettinga, S. Rebac, G. Zeeman, Challenge of psychrophilic anaerobic wastewater treatment, Trends Biotechnol. 19 (2001) 363–370.

[8] J. Gouveia, F. Plaza, G. Garralon, F. Fdz-Polanco, M. Peña, Long-term operation of a pilot scale anaerobic membrane bioreactor (AnMBR) for the treatment of municipal wastewater under psychrophilic conditions, Bioresour. Technol. 185 (2015) 225–233.

[9] B.Q. Liao, J.T. Kraemer, D.M. Bagley, Anaerobic membrane bioreactors: applications and research directions, Crit. Rev. Environ. Sci. Technol. 36 (2006) 489–530.

[10] A.L. Smith, S.J. Skerlos, L. Raskin, Psychrophilic anaerobic membrane bioreactor treatment of domestic wastewater, Water Res. 47 (2013) 1655–1665.

[11] I. Martin-Garcia, V. Monsalvo, M. Pidou, P. Le-Clech, S.J. Judd, E.J. McAdam, B. Jefferson, Impact of membrane configuration on fouling in anaerobic membrane bioreactors, J. Memb. Sci. 382 (2011) 41–49.

[12] R. Pretel, A. Robles, M.V. Ruano, A. Seco, J. Ferrer, The operating cost of an anaerobic membrane bioreactor (AnMBR) treating sulphate-rich urban wastewater, Sep. Purif. Technol. 126 (2014) 30–38.

[13] L. Vera, E. González, I. Ruigómez, J. Gómez, S. Delgado, Influence of gas sparging intermittence on ultrafiltration performance of anaerobic suspensions, Ind. Eng. Chem. Res. 55 (2016) 4668–4675.

[14] J. Cookney, A. Mcleod, V. Mathioudakis, P. Ncube, A. Soares, B. Jefferson, E.J. McAdam, Dissolved methane recovery from anaerobic effluents using hollow fibre membrane contactors, J. Memb. Sci. 502 (2016) 141–150.

[15] J. Gouveia, F. Plaza, G. Garralon, F. Fdz-Polanco, M. Peña, A novel configuration for an anaerobic submerged membrane bioreactor (AnSMBR), Bioresour. Technol. 198 (2015) 510–519.

[16] C. Shin, P.L. McCarty, J. Kim, J. Bae, Pilot-scale temperate-climate treatment of domestic wastewater with a staged anaerobic fluidized membrane bioreactor (SAF-MBR), Bioresour. Technol. 159 (2014) 95–103.

[17] S.J. Judd, Principles and Applications of Membrane Bioreactors in Water and Wastewater Treatment, 2nd ed., Elsevier, London,UK, 2011.

[18] Y. Wibisono, E.R. Cornelissen, A.J.B. Kemperman, W.G.J. Van Der Meer, K. Nijmeijer, Two-phase flow in membrane processes: A technology with a future, J. Memb. Sci. 453 (2014) 566–602.

[19] D. Martinez-Sosa, B. Helmreich, T. Netter, S. Paris, F. Bischof, H. Horn, Anaerobic submerged membrane bioreactor (AnSMBR) for municipal wastewater treatment under mesophilic and psychrophilic temperature conditions, Bioresour. Technol. 102 (2011) 10377–10385.

[20] Q. Dong, W. Parker, M. Dagnew, Impact of FeCl3 dosing on AnMBR treatment of municipal wastewater., Water Res. 80 (2015) 281–293.

[21] E. van Voorthuizen, A. Zwijnenburg, W. van der Meer, H. Temmink, Biological black water treatment combined with membrane separation, Water Res. 42 (2008) 4334–4340.

[22] H. Ozgun, Y. Tao, M.E. Ersahin, Z. Zhou, J.B. Gimenez, H. Spanjers, J.B. van Lier, Impact of temperature on feed-flow characteristics and filtration performance of an upflow anaerobic sludge blanket coupled ultrafiltration membrane treating municipal wastewater, Water Res. 83 (2015) 71–83.

[23] B.D. Cho, A.G. Fane, Fouling transients in nominally sub-critical flux operation of a membrane bioreactor, J. Memb. Sci. 209 (2002) 391–403.

[24] E.J. McAdam, S.J. Judd, Optimisation of dead-end filtration conditions for an immersed anoxic membrane bioreactor, J. Memb. Sci. 325 (2008) 940–946.

[25] E.J. McAdam, E. Cartmell, S.J. Judd, Comparison of dead-end and continuous filtration conditions in a denitrification membrane bioreactor, J. Memb. Sci. 369 (2011) 167–173.

[26] S. Aiyuk, I. Forrez, D.K. Lieven, A. van Haandel, W. Verstraete, Anaerobic and complementary treatment of domestic sewage in regions with hot climates-A review, Bioresour. Technol. 97 (2006) 2225–2241.

[27] S. Chong, T.K. Sen, A. Kayaalp, H.M. Ang, The performance enhancements of upflow anaerobic sludge blanket (UASB) reactors for domestic sludge treatment - A State-of-the-art review, Water Res. 46 (2012) 3434–3470.

[28] S. Delgado, R. Villarroel, E. González, Effect of the shear intensity on fouling in submerged membrane bioreactor for wastewater treatment, J. Memb. Sci. 311 (2008) 173–181.

[29] P. Le-Clech, B. Jefferson, S.J. Judd, A comparison of submerged and sidestream tubular membrane bioreactor configurations, Desalination. 173 (2005) 113–122.

[30] G. Guglielmi, D. Chiarani, S.J. Judd, G. Andreottola, Flux criticality and sustainability in a hollow fibre submerged membrane bioreactor for municipal wastewater treatment, J. Memb. Sci. 289 (2007) 241–248.

[31] L. Vera, E. González, I. Ruigómez, J. Gómez, S. Delgado, Analysis of backwashing efficiency in dead-end hollow-fibre ultrafiltration of anaerobic suspensions, Environ. Sci. Pollut. Res. 22 (2015) 16600–16609.

[32] L. Vera, E. Gonzalez, O. Diaz, R. Sanchez, R. Bohorque, J. Rodriguez-Sevilla, Fouling analysis of a tertiary submerged membrane bioreactor operated in dead-end mode at high-fluxes, J. Memb. Sci. 493 (2015) 8–18.

[33] A.A. McCarty, P. Gilboy, P.K. Walsh, G. Foley, Characterisation of cake compressibility in dead-end microfiltration of microbial suspensions, Chem. Eng. Commun. 173 (1999) 79–90.

[34] APHA, Standard Methods for the Examination of Water and Wastewater, 21st ed., American Public Health Association, Washington D.C, 2005.

[35] W. Parawira, M. Murto, J.S. Read, B. Mattiasson, Volatile fatty acid production during anaerobic mesophilic digestion of solid potato waste, J. Chem. Technol. Biotechnol. 79 (2004) 673–677.

[36] O.H. Lowery, N.J. Rosebrough, A.L. Farr, R.J. Randall, Protein measurement with the folin phenol reagent, J. Biol. Chem. 193 (1951) 265–275.

[37] M. Dubois, K.A. Gilles, J.K. Hamilton, P.A. Rebers, F. Smith, Colorimetric method for determination of sugars and related substances, Anal. Chem. 28 (1956) 350–356.

[38] J. Krompcamp, F. Faber, K. Schroen, R. Boom, Effects of particle size segregation on crossflow microfiltration performance: Control mechanism for concentration polarisation and particle fractionation, J. Memb. Sci. 268 (2006) 189–197.

[39] E. Tardieu, A. Grasmick, V. Geaugey, J. Manem, Hydrodynamic control of bioparticle deposition in a MBR applied to wastewater treatment, J. Memb. Sci. 147 (1998) 1–12.

[40] S.H. Yoon, Membrane Bioreactor Processes: Principles and Applications, CRC press, 2015.

[41] F. Fan, H. Zhou, Interrelated effects of aeration and mixed liquor fractions on membrane fouling for submerged membrane bioreactor processes in wastewater treatment, Environ. Sci. Technol. 41 (2007) 2523–2528.

[42] T. Buer, J. Cumin, MBR module design and operation, Desalination. 250 (2010) 1073–1077.

[43] D. Guibert, R.B. Aim, H. Rabie, P. Côté, Aeration performance of immersed hollow-fiber membranes in a bentonite suspension, Desalination. 148 (2002) 395–400.

[44] P. Harmant, P. Aimar, Coagulation of colloids retained by porous wall, AIChE J. 42 (1996) 3523–3532.

[45] Y. Bessiere, N. Abidine, P. Bacchin, Low fouling conditions in dead-end filtration: Evidence for a critical filtered volume and interpretation using critical osmotic pressure, J. Memb. Sci. 264 (2005) 37–47.

[46] F. Meng, H. Zhang, F. Yang, Y. Li, J. Xiao, X. Zhang, Effect of filamentous bacteria on membrane fouling in submerged membrane bioreactor, J. Memb. Sci. 272 (2006) 161–168.

[47] H. Hong, M. Zhang, Y. He, J. Chen, H. Lin, Fouling mechanisms of gel layer in a submerged membrane bioreactor, Bioresour. Technol. 166 (2014) 295–302.

[48] B. Verrecht, T. Maere, I. Nopens, C. Brepols, S. Judd, The cost of a large-scale hollow fibre MBR, Water Res. 44 (2010) 5274–5283.

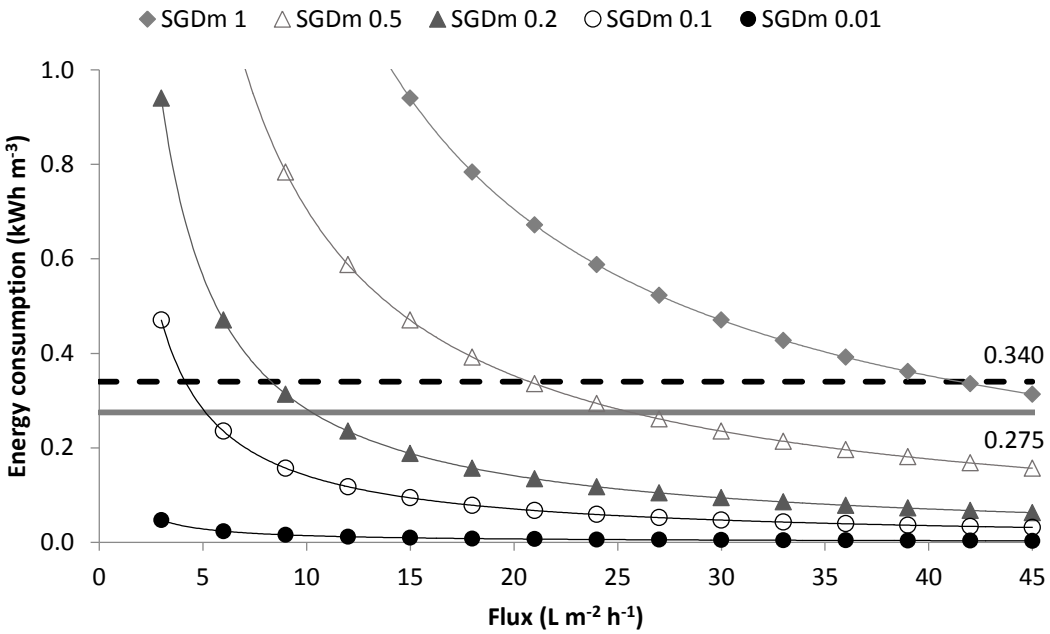

Figure 1. Energy consumption of AnMBR for different fluxes and specific gas demand per unit membrane area (SGD_m). Data compared to energy recovered from this sewage using AnMBR (0.275 kWh m^{-3}, biogas from UASB and dissolved CH_4) [14]. Black break line illustrates average energy recovery from municipal AnMBR literature (0.34 kWh m^{-3}) [8,14–16].

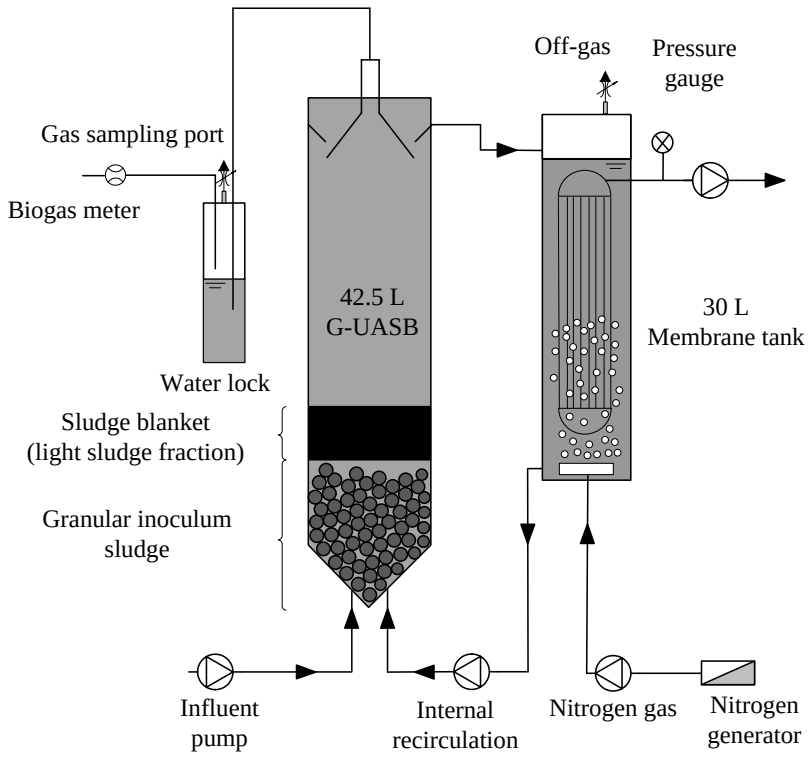

Figure 2. Schematic of the anaerobic membrane bioreactor (AnMBR).

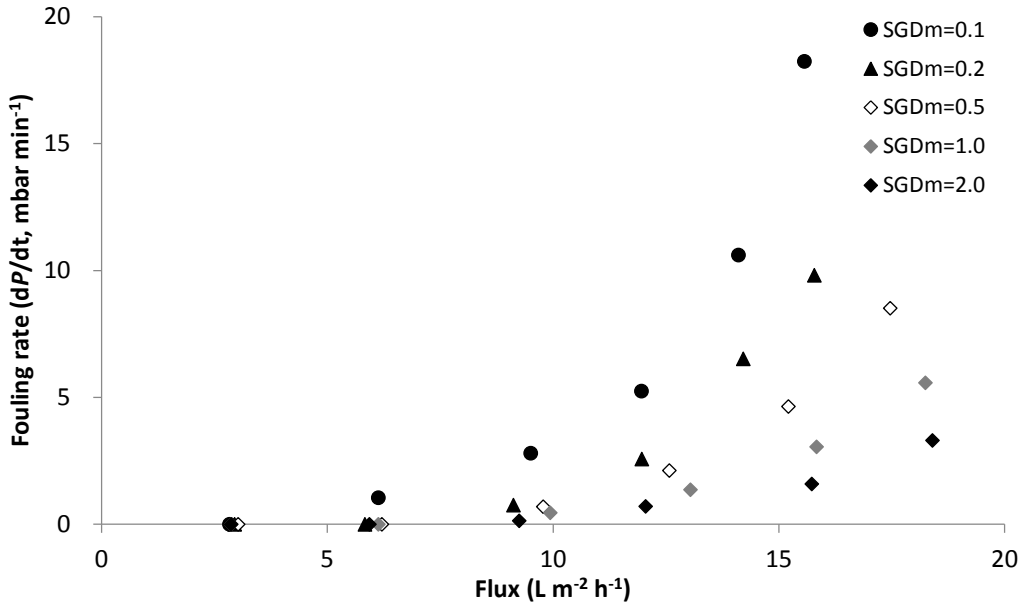

Figure 3. Critical flux determination under different specific gas demand per unit membrane area (SGD_m) (3 L m^{-2} h^{-1} per step; 10 mins step).

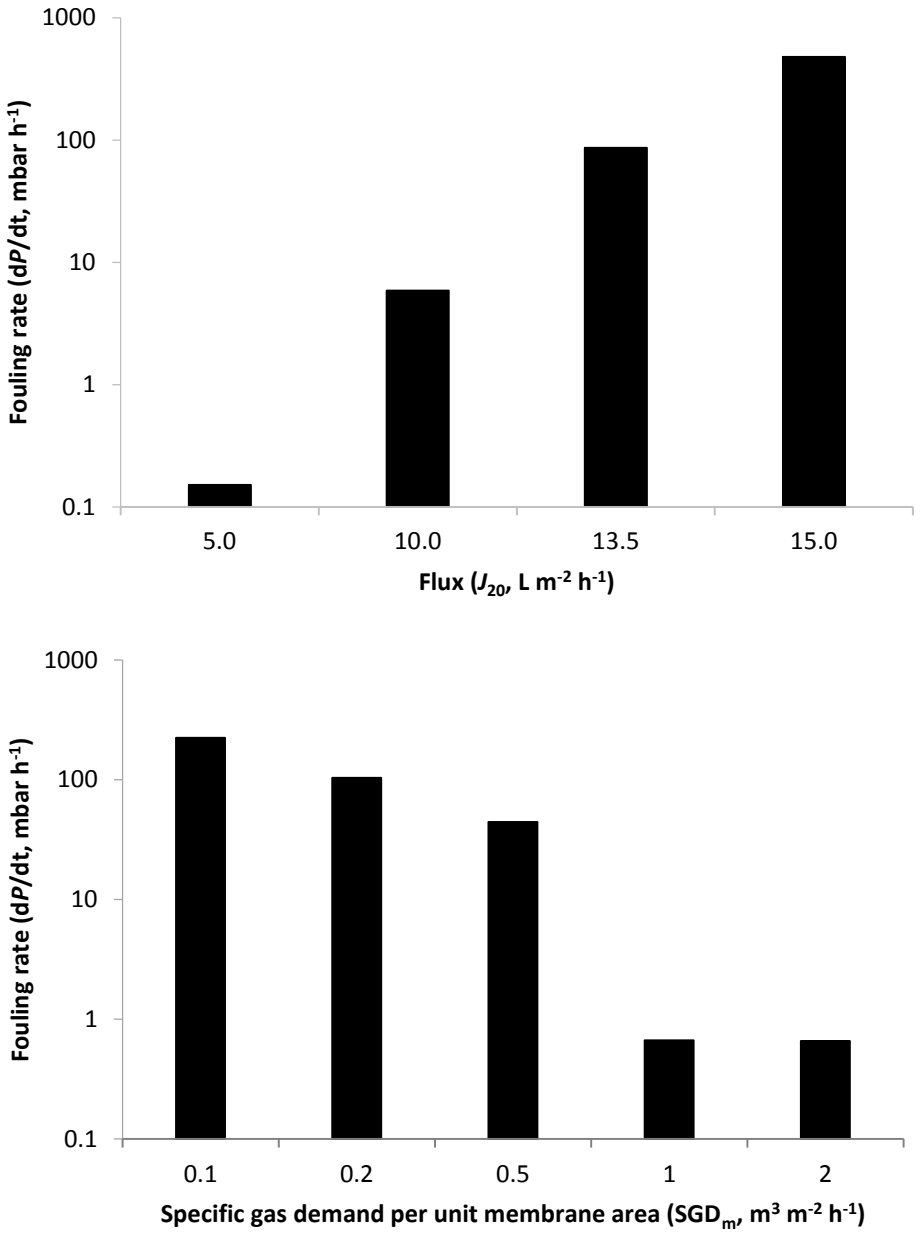

Figure 4. Impact of flux (specific gas demand per unit membrane area (SGD_m), 0.2 m^3 m^{-2} h^{-1}) and SGD_m (fixed flux, J_{20} =13.5 L m^{-2} h^{-1}) on membrane fouling rate using continuous filtration and continuous gas sparging. Filtration to 24 h or TMP_{max} (550 mbar).

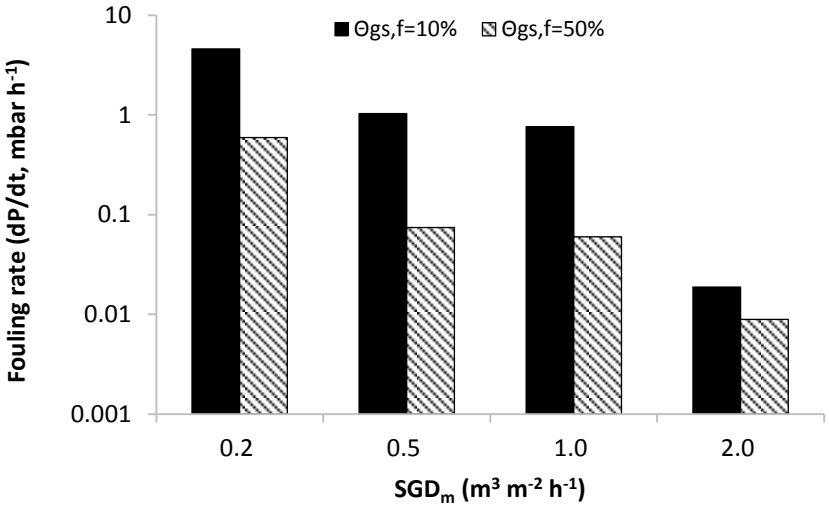

(a)

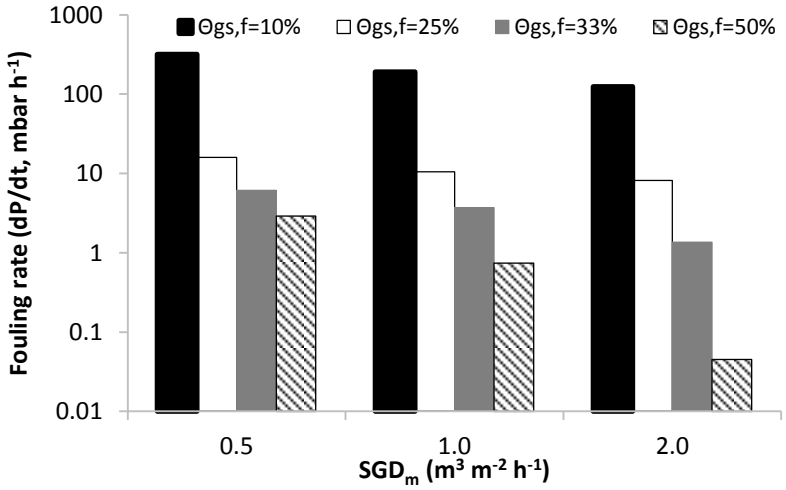

(b)

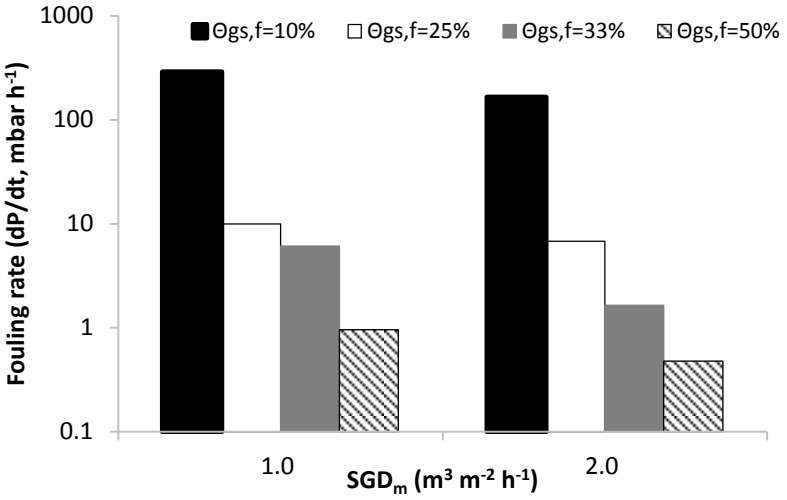

(c)

Figure 5. Impact of specific gas demand per unit membrane area (SGD_m) and gas sparging frequency ($\Theta_{gs,f}$) (10 s on time fixed) on membrane fouling rate using continuous filtration and intermittent gas sparging: (a) J_{20}= 5 L m^{-2} h^{-1}; (b) 10 L m^{-2} h^{-1}; (c) 13.5 L m^{-2} h^{-1}. Filtration to 24 h or TMP_{max} (550 mbar).

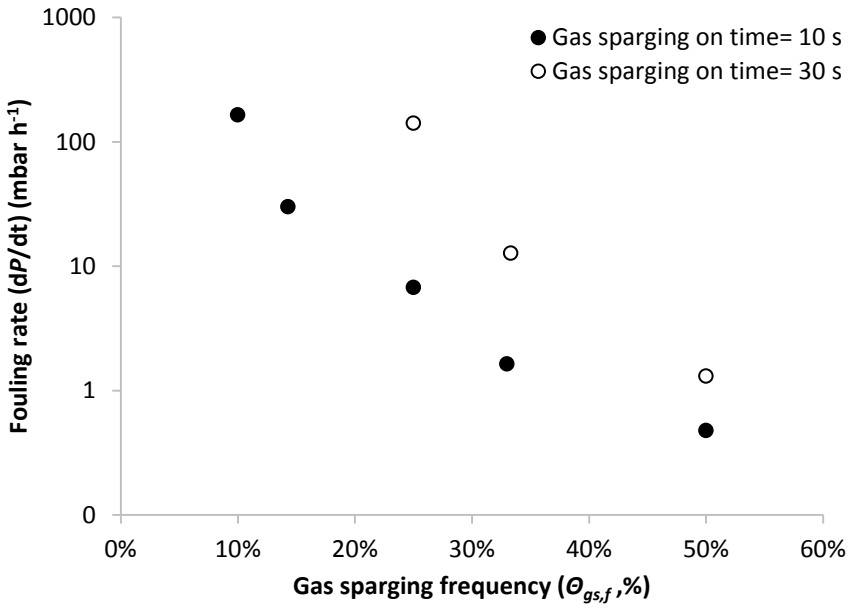

Figure 6. Impact of gas sparging frequency ($\Theta_{gs,f}$) and gas sparging on time ($\theta_{gs,on}$) on membrane fouling rate using continuous filtration and intermittent gas sparging at fixed flux (J_{20}=13.5 L m^{-2} h^{-1}, SGD_m=2.0 m^3 m^{-2} h^{-1}). Filtration to 24 h or TMP_{max} (550 mbar).

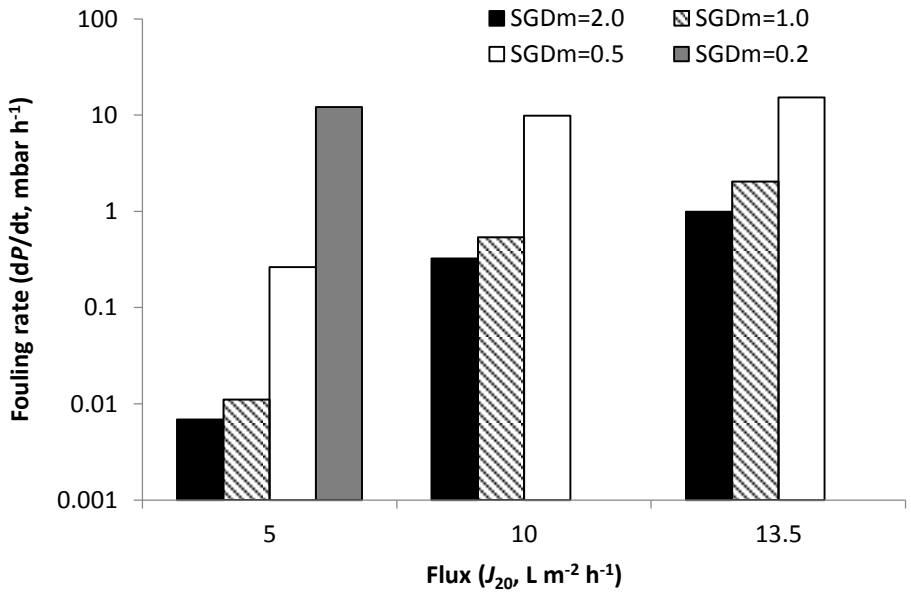

Figure 7. Impact of specific gas demand per unit membrane area (SGD_m) on membrane fouling rate using dead-end gas sparging regime: 9 min on/1 min off; $J_{20\ net}$= 5, 10, 13.5 L m^{-2} h^{-1}. Gas sparging introduced once filtration has stopped. Filtration to 24 h or TMP_{max} (550 mbar).

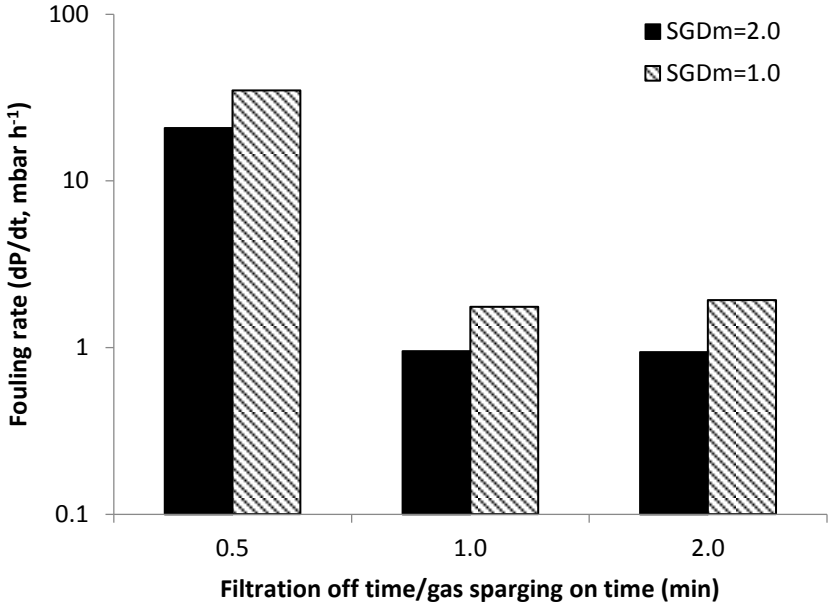

(a)

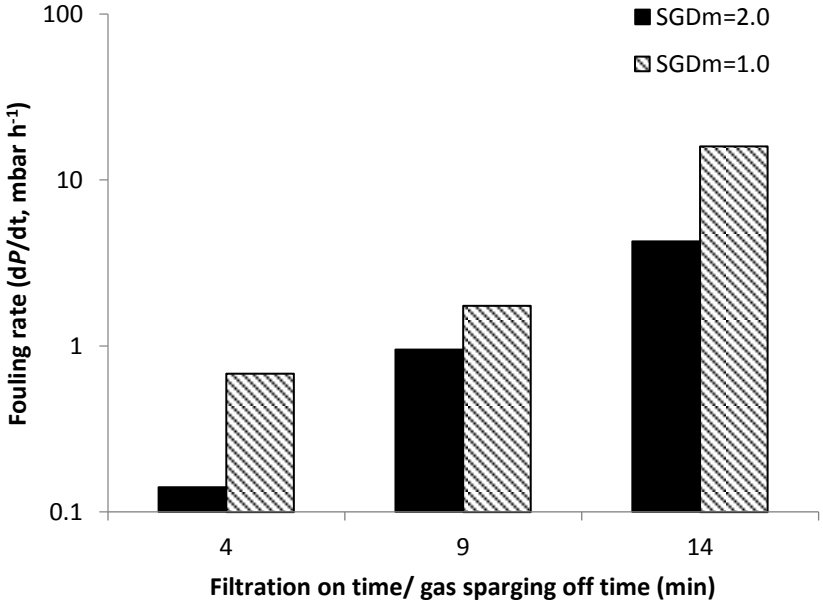

(b)

Figure 8. Impact of filtration off time (gas sparging on time) and filtration on time (gas sparging off time) on membrane fouling rate using dead-end gas sparging regime (J_{20}=13.5 L m^{-2} h^{-1}, $J_{20\ net}$ varied): (a) fixed filtration off time (1 min); (b) fixed filtration on time (9 min). Filtration to 24 h or TMP_{max} (550 mbar).

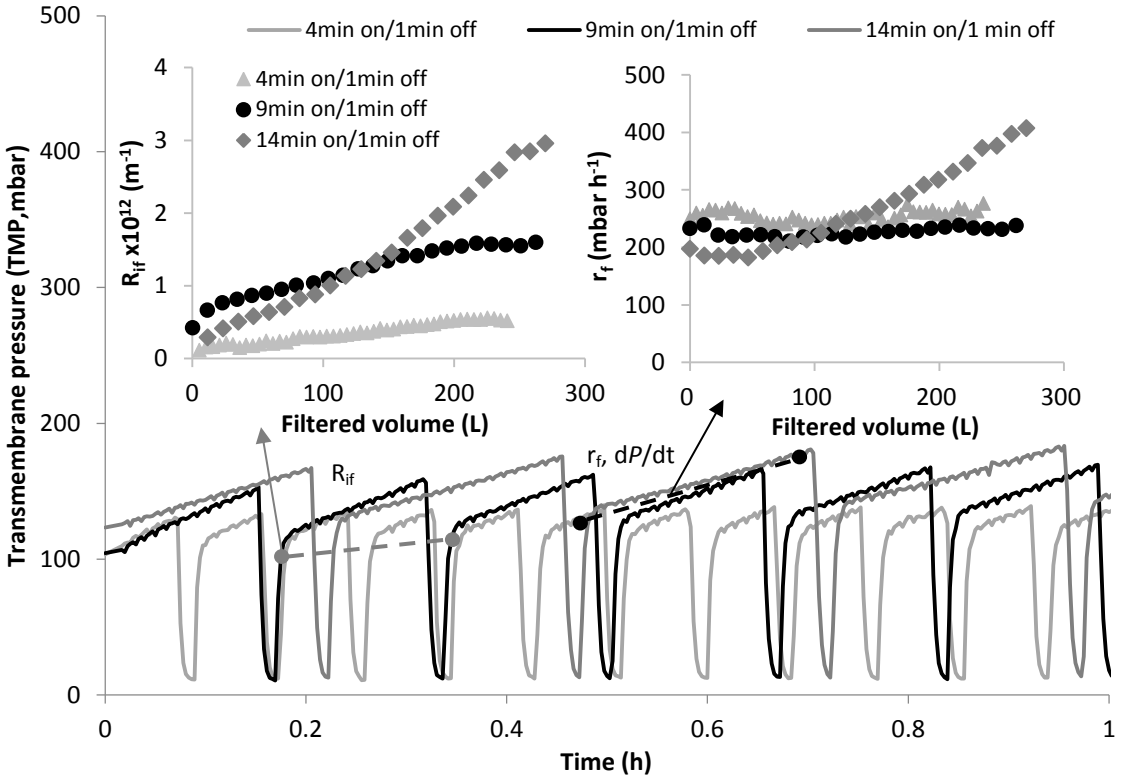

Figure 9. Internal residual fouling resistance (R_{if}, calculated from pressure at onset of filtration) and cake fouling rate (r_f, dP/dt) analyses under dead-end gas sparging regime. J_{20}, 13.5 L m^{-2} h^{-1}; filtration 4min on/1min off, 9min on/1min off, 14min on/1 min off. Gas sparging introduced once filtration has stopped: SGD_m, 2.0 m^3 m^{-2} h^{-1}.

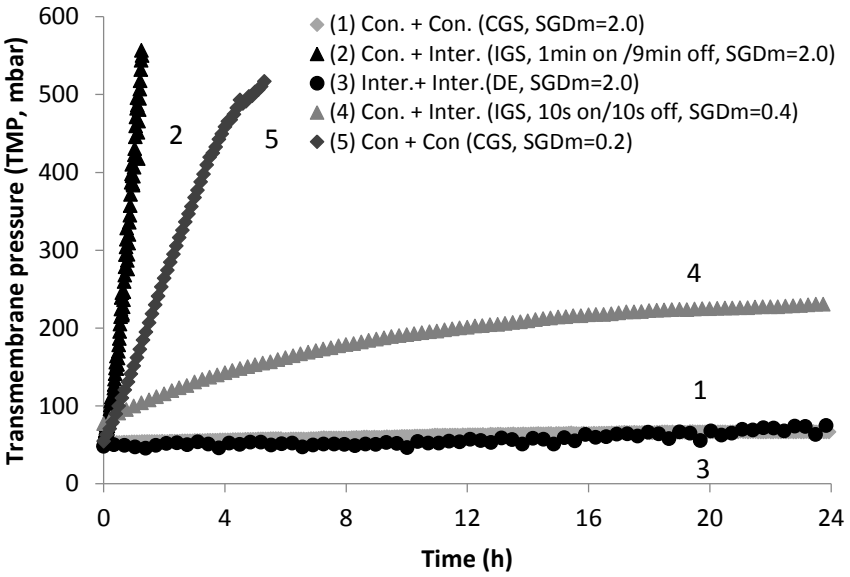

Figure 10. Comparison of membrane fouling under same specific gas demand per membrane area (SGD_m) and same net SGD_m ($SGD_{m\ net}$) with different gas sparging regimes ($J_{20\ net}$= 13.5 L m^{-2} h^{-1}). Con. (Continuous), Inter. (Intermittent); CGS (continuous gas sparging), IGS (intermittent gas sparging), DE (dead-end gas sparging). Detailed test parameters can be referred to Table 2.

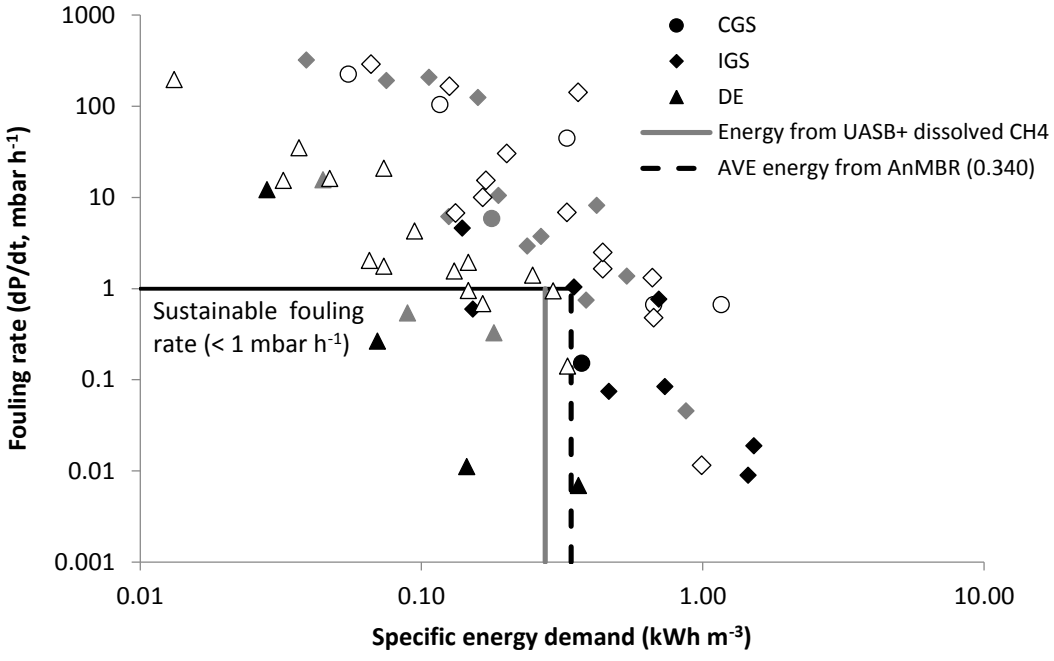

Figure 11. Impact of specific energy demand on membrane fouling (based on 3 m hydraulic head). CGS, continuous gas sparging; IGS, intermittent gas sparging; DE, dead-end. Black, grey and white data represent fluxes (J_{20}) of: 5, 10 and 13.5 L m^{-2} h^{-1}. Lines represent energy recovered from biogas and dissolved CH_4 using: sewage from the present study (grey solid line) [14]; average from the municipal AnMBR literature (black broken line) [8,14–16].

Table 1 Influent characteristics, G-AnMBR treatment performance and bulk sludge characteristics

Parameter	Unit	Influent	Membrane tank	Permeate	Removal %
pH	-	7.8±0.3 (n=181)	7.9±0.3 (n=165)	8.2±0.2 (n=80)	-
MLSS	mg L^{-1}	131±38 (n=181)	384±190 (n=156)	<DL	>99
COD_t	mg L^{-1}	221±78 (n=175)	663±333 (n=151)	41±16 (n=74)	83±7
BOD_5	mg L^{-1}	106±39 (n=39)	-	11±7 (n=42)	90±6
SCOD	mg L^{-1}	88±30 (n=174)	149±65 (n=153)	41±16 (n=74)	-
SMP_P	mg L^{-1}	39±9 (n=117)	59±19 (n=129)	-	-
SMP_C	mg L^{-1}	7±3 (n=117)	19±11 (n=137)	-	-
SMP P/C	-	6.1±2.7 (n=116)	3.8±1.7 (n=136)	-	-
Particle size (d_{50})	µm	64±24 (n=96)	62±45 (n=112)	-	-
VFA	mg CH_3COOH L^{-1}	22.8±14.8 (n=26)	-	<2.0[a] (n=18)	-

a. limit of detection (LOD), 2.0 mg L^{-1}
DL-detection limit

Table 2 Comparison of different gas sparging regimes under same specific gas demand per membrane area (SGD_m) and same net SGD_m ($SGD_{m\ net}$).

	Filtration	Gas sparging	Filtration On/Off min	Gas sparing On/Off min	J_{20}[a] L m^{-2} h^{-1}	$J_{20\ net}$[b] L m^{-2} h^{-1}	SGD_m m^3 m^{-2} h^{-1}	$SGD_{m\ net}$ m^3 m^{-2} h^{-1}	Energy demand kWh m^{-3}
1	Con.	Con. (CGS)	-	-	13.5	13.5	2	2	1.325
2	Con.	Inter.(IGS)	-	1min/9min	13.5	13.5	2	0.2	0.133
3	Inter.	Inter. (DE)	9min/1min	1min/9min	15	13.5	2	0.2	0.133
4	Con.	Inter. (IGS)	-	10s/10s	13.5	13.5	0.4	0.2	0.133
5	Con.	Con. (CGS)	-	-	13.5	13.5	0.2	0.2	0.133

a. J_{20}, flux at 20°C; b. $J_{20\ net}$, net flux at 20°C
Con. (Continuous), Inter. (Intermittent); CGS (continuous gas sparging), IGS (intermittent gas sparging), DE (dead-end gas sparging)